Chapter

Fast Indicators for Orbital Stability: A Survey on Lyapunov and Reversibility Errors

Giorgio Turchetti and Federico Panichi

Abstract

We present a survey on the recently introduced fast indicators for Hamiltonian systems, which measure the sensitivity of orbits to small initial displacements, Lyapunov error (LE), and to a small additive noise, reversibility error (RE). The LE and RE are based on variational methods and require the computation of the tangent flow or map. The modified reversibility error method (REM) measures the effect of roundoff and is computed by iterating a symplectic map forward and backward the same number of times. The smoothest indicator is RE since it damps the oscillations of LE. It can be proven that LE and RE grow following a power law for regular orbits and an exponential law for chaotic orbits. There is a numerical evidence that the growth of RE and REM follows the same law. The application to models of celestial and beam dynamics has shown the reliability of these indicators.

Keywords: variational principles, reversibility error, additive noise, roundoff

1. Introduction

The global stability properties of Hamiltonian systems and symplectic maps have a solid theoretical foundation [1, 2]. Nevertheless, the determination of the orbital stability by computing the maximum Lyapunov exponent is a procedure difficult to implement numerically, because of the $t \to \infty$ limit. For this reason a variety of fast indicators has been developed during the last two decades [3–7]. The variational methods mentioned above measure the sensitivity to initial conditions of the orbit computed for finite times. The spectral methods [8, 9] relate the stability to the behavior of the Fourier spectrum of the orbit computed for finite times.

In the framework of the variational methods, we have proposed two indicators [10–12] the Lyapunov error (LE) and the reversibility error (RE) introducing also the modified reversibility error method (REM). The LE is due to a small displacement of the initial condition, the RE is due to an additive noise, and REM is due to roundoff. The reversibility error due to the roundoff or noise is more convenient with respect to the error occurring in the forward evolution of the map.[1]

[1] The forward error (FE) due to additive noise in the forward evolution of a map can be defined and written in terms of the tangent map. However, RE is very simply related to LE, whereas FE is not. In addition the error due to roundoff in the forward evolution requires in principle the evaluation of the exact orbit or, in practice, its evaluation with a much higher accuracy.

In the limit of a vanishing amplitude of the initial displacement or of the random displacement, the LE and RE are defined by using the tangent map along the orbit. Furthermore, RE is related to LE by a very simple formula. A reversibility error is always present in numerical computations due to roundoff even when no additive noise is introduced. We compute REM by iterating n times the map M, then its inverse n times, and dividing the norm of the displacement from the initial point, by the roundoff amplitude. The procedure is extremely simple and does not require the knowledge of the tangent map. Though the effect of roundoff on a single iteration is not equivalent to a random displacement, after many iterations the cumulative result is comparable if the computational complexity of the map is sufficiently high. The main difference is that for an additive noise, the error is defined as the root mean square deviation of the noisy orbit with respect to the exact one, obtained by averaging over all possible realizations of the noise, whereas for the roundoff a unique realization is available. As a consequence REM fluctuates with the iteration number n, whereas RE does not. A statistical analysis of roundoff compared to a random noise was previously performed using the fidelity method [13, 14], and a comparison of REM with other fast indicators was initially carried out for the standard map [15]. The growth of errors, for REM-, RE-, and Lyapunov-based indicators, is governed by the tangent map. For LE a small initial displacement is propagated and amplified along the orbit. For RE or REM, a random or pseudorandom displacement is introduced at any (forward or backward) iteration of the map and is propagated and amplified along the orbit. The final random displacement is the sum of the global displacements triggered by the local displacements (due to noise or roundoff) occurring at any iteration. Therefore, it is not surprising that the square of RE is twice the sum of the squares of LE computed along the orbit and that all the numerical experiments suggest that REM exhibits a similar behavior even though with larger fluctuations.

For an integrable map, the growth of LE and RE follows asymptotically a power law n^α, and the exact analytical result is known. This result can be extended to quasi integrable maps by using the normal forms theory. For uniformly chaotic maps (hyperbolic automorphisms of the torus), the LE and RE have an exponential growth $e^{\lambda n}$. For generic maps, the asymptotic growth of LE and RE follows a power law in the regions of regular motion and an exponential law in the regions of chaotic motion, and the same behavior is observed for REM. For an integrable or quasi integrable map, LE has an asymptotic linear growth $\alpha = 1$ with oscillations, whereas RE has an asymptotic power law growth with $\alpha = 3/2$ without oscillations, since they are rapidly damped. The oscillations of LE disappear when the map is written in normal coordinates. For a linear map conjugated to a rotation, the power law exponents are $\alpha = 0$ for LE and $\alpha = 1/2$ for RE. For REM the power law exponent α varies between 0 and 1, its value depending on the computational complexity of the map and therefore on the choice of coordinates.

The definition of LE we propose differs from fast Lyapunov indicator (FLI) [3] or orthogonal fast Lyapunov indicator (OFLI) [4], which are based on the growth along the orbit of the norm of a given initial displacement vector. Indeed, we compute the growth of the vectors of an orthogonal basis, which amounts to defining LE, which we denote as e_n^L, as the square root of $\mathrm{Tr}\left(\left(DM^n(\mathbf{x}_0)\right)^T DM^n(\mathbf{x}_0)\right)$ where $M(\mathbf{x})$ is the map, $DM(\mathbf{x})$ denotes the tangent map, and $\mathbf{x}_0$ is the initial condition. This definition has the obvious advantage of insuring the correct asymptotic growth.

Indeed the anomalies in the behavior of FLI [16], due to the choice of the initial vector, are not met. The use of exponential growth factor of nearby orbits (MEGNO) [17] allows to filter the oscillations which are still present in LE. The RE

is obtained from the covariance matrix which is computed from the tangent map. We denote this error by e_n^R, which has a very simple relation with LE given by the square root of $\left(e_0^L\right)^2 + 2\left(e_1^L\right)^2 + \ldots + 2\left(e_{n-1}^L\right)^2 + \left(e_n^L\right)^2$. We first analyze the case of linear maps to explore the behavior of REM. A systematic comparison of LE, RE, and REM is presented for two basic models: the standard map and the Hénon map. The asymptotic power law exponents are computed by using the MEGNO filter. For nonlinear two-dimensional maps, the behavior of the errors has been compared moving along a one-dimensional grid in the phase plane: crossing of islands has a clear signature, the chaotic regions are very neatly distinguished, and good agreement with the theoretical predictions is found.

A rectangular region of phase plane has been examined by choosing a grid and using a color, logarithmic scale for the errors at each point. Also in this case, a good correspondence with the phase space portrait is found. On the basis of the analysis presented here and the experience gained in investigating more complex models from celestial mechanics [18] and beam dynamics [19], we suggest to compare RE and REM with LE, possibly, filtered with MEGNO, to damp the oscillations[2]. For maps of dimension 4 or higher, a direct geometric inspection of the orbits is not possible since the Poincaré section requires an interpolation Hamiltonian. As a consequence the use of fast indicators is the only practical approach to analyze the orbital stability. Hamiltonian systems have a continuous time flow, and the errors LE and RE denoted by $e^L(t)$ and $e^R(t)$, respectively, are computed by using the fundamental matrix $\mathrm{L}(t)$ of the tangent flow. In this case $e_L(t) = \left(\mathrm{Tr}\left(\mathrm{L}^T(t)\,\mathrm{L}(t)\right)\right)^{1/2}$ and $e^R(t)$ are given by the square root of $2\int_0^t ds\left(e^L(s)\right)^2$, whose trapezoidal rule approximation gives the relation found for the maps [12]. Standard procedures allow to approximate the orbit $\mathbf{x}(t)$ by the iterates $M^n(\mathbf{x}_0)$ of a symplectic integrator map M (see [20]) and the fundamental matrix $\mathrm{L}(t)$ by $DM^n(\mathbf{x}_0)$ (see [21]). The paper has the following structure. In Section 2, we recall the definitions for LE and RE and obtain their mutual relation. In Section 3, we present the analytical results on LE and RE together with the numerical results on REM for integrable maps. In Section 4, the key features of two prototype models, the standard map and the Hénon map, are summarized. In Section 5, we present a detailed numerical analysis of LE, RE, and REM for the standard map. In Section 6, the same analysis is presented for the Hénon map. In Section 7, the summary and conclusions are presented.

2. Definition of errors

Given a symplectic map $M(\mathbf{x})$ where $\mathbf{x} \in \mathbb{R}^{2d}$, we consider the orbits $\mathbf{x}_n = M^n(\mathbf{x}_0)$ and $\mathbf{y}_n = M^n\left(\mathbf{y}_0\right)$ for two initial points $\mathbf{x}_0$ and $\mathbf{y}_0 = \mathbf{x}_0 + \epsilon\boldsymbol{\eta}_0$, respectively, where $\boldsymbol{\eta}$ is a unit vector. We consider the normalized displacement $\boldsymbol{\eta}_n$ at iteration n defined by

$$\boldsymbol{\eta}_n = \lim_{\epsilon \to 0} \frac{\mathbf{y}_n - \mathbf{x}_n}{\epsilon} = \lim_{\epsilon \to 0} \frac{M\left(\mathbf{y}_{n-1}\right) - M(\mathbf{x}_{n-1})}{\epsilon} \tag{1}$$

[2] The application of MEGNO to RE is not necessary due to the absence of oscillations, whereas its application to REM is not recommended because the fluctuations are not filtered and the computational cost is quadratic rather than linear in the iteration order.

which satisfies the linear recurrence

$$\boldsymbol{\eta}_n = DM(\mathbf{x}_{n-1})\boldsymbol{\eta}_{n-1} \qquad (DM)_{ij} = \frac{\partial M_i}{\partial x_j} \tag{2}$$

where DM is the tangent map. For any finite ϵ, we have $\mathbf{y}_n = \mathbf{x}_n + \epsilon\boldsymbol{\eta}_n + O(\epsilon^2)$. We might define the error as the norm of $\boldsymbol{\eta}_n$ which is closely related to the fast Lyapunov indicator FLI (see [3]) as

$$e_n(\boldsymbol{\eta}_0) = \|\boldsymbol{\eta}_n\| = \|DM^n(\mathbf{x}_0)\boldsymbol{\eta}_0\| \qquad (FLI)_n = \max_{1\le k\le n} \log e_k(\boldsymbol{\eta}_0) \tag{3}$$

and to its variants such as OFLI [4]. The mean exponential growth factor of nearby orbits, MEGNO [17], denoted by $Y_n = Y(e_n)$ is the double average of the slope, and we denote it as Δe_n^2. When n is a continuous variable, then $\Delta e_n^2 = d\log e_n^2/d\log n$. When n is an integer, the standard definition is

$$\Delta e_n^2 = n\left(\log e_n^2 - \log e_{n-1}^2\right) \qquad Y_n = \left\langle\left\langle \Delta e_n^2 \right\rangle\right\rangle. \tag{4}$$

2.1 Lyapunov error

We propose a definition of the Lyapunov error which is independent from the choice of the initial vector:

$$\begin{aligned} e_n^L &= \left(\mathrm{Tr}\left(\mathrm{A}_n^T\mathrm{A}_n\right)\right)^{1/2} \\ \mathrm{A}_n &= DM^n(\mathbf{x}_0) = DM(\mathbf{x}_{n-1})\mathrm{A}_{n-1} \qquad \mathrm{A}_0 = \mathrm{I} \end{aligned} \tag{5}$$

It is immediate to verify that given an orthonormal basis $\boldsymbol{\eta}_{0k}$, we have

$$e_n^L = \left(\sum_{k=1}^{2d} e_n^2(\boldsymbol{\eta}_{0k})\right)^{1/2} \tag{6}$$

and obviously the result does not depend on the choice of the basis. The computational cost of $e_n(\boldsymbol{\eta}_0)$ is $2d$ times higher with respect to e_n^L, but this difference is negligible with respect to the computational cost of the matrix $DM(\mathbf{x}_{n-1})$, which recursively gives $\boldsymbol{\eta}_n$ and A_n. A similar definition is proposed in the case of Hamiltonian flows (see the last Subsection 2.6 and [12] for more details). An advantage of the proposed definition is that it takes into account the error growth on all possible directions of the initial displacement vector. As a consequence, no spurious effects due to the choice of the initial vector have to be faced (see [16]).

2.2 Forward error

When an additive noise of amplitude ϵ is introduced, the reference orbit $\mathbf{x}_n$ is replaced by the noisy one ($\mathbf{y}_n$) having the same initial condition:

$$\mathbf{y}_n = M(\mathbf{y}_{n-1}) + \epsilon\boldsymbol{\xi}_n \qquad \mathbf{y}_0 = \mathbf{x}_0 \tag{7}$$

where $\boldsymbol{\xi}_n$ are independent random vectors satisfying

$$\langle\boldsymbol{\xi}_n\rangle = 0 \qquad \left\langle\boldsymbol{\xi}_n\boldsymbol{\xi}_m^T\right\rangle = \mathrm{I}\,\delta_{nm} \tag{8}$$

The global stochastic displacement satisfies a linear nonhomogeneous equation and is defined by

$$\boldsymbol{\Xi}_n = \lim_{\epsilon \to 0} \frac{\mathbf{y}_n - \mathbf{x}_n}{\epsilon} \qquad \boldsymbol{\Xi}_n = DM(\mathbf{x}_{n-1})\boldsymbol{\Xi}_{n-1} + \boldsymbol{\xi}_n \tag{9}$$

with initial condition $\boldsymbol{\Xi}_0 = 0$. Letting $\Sigma_n^{2F} = \left\langle \boldsymbol{\Xi}_n \boldsymbol{\Xi}_n^T \right\rangle$ be the covariance matrix the forward error is defined by

$$e_n^F = \left\langle \boldsymbol{\Xi}_n \cdot \boldsymbol{\Xi}_n \right\rangle^{1/2} = \left(\mathrm{Tr}\left(\Sigma_n^{2F} \right) \right)^{1/2} \tag{10}$$

The explicit solution for $\boldsymbol{\Xi}_n$ is given by

$$\boldsymbol{\Xi}_n = \sum_{k=1}^{n} DM^{n-k}(\mathbf{x}_k)\,\boldsymbol{\xi}_k = \sum_{k=0}^{n-1} \mathrm{B}_k\,\boldsymbol{\xi}_{n-k} \qquad \mathrm{B}_k = DM^k(\mathbf{x}_{n-k}) \tag{11}$$

where B_k can be evaluated recursively as

$$\mathrm{B}_k = \mathrm{B}_{k-1} DM(\mathbf{x}_{n-k}) \qquad \mathrm{B}_0 = \mathrm{I}. \tag{12}$$

The expression for the forward error finally reads

$$e_n^F = \left(\sum_{k=0}^{n-1} \mathrm{Tr}\left(\mathrm{B}_k^T \mathrm{B}_k \right) \right)^{1/2}. \tag{13}$$

The computation cost of B_n is negligible, once we have evaluated the tangent map, but the storage of the tangent map along the orbit up to n is required.

2.3 Reversibility error

We have just defined the forward error, but it will not be used, because it is only an intermediate step toward the definition of the reversibility error. Consider the backward evolution $\mathbf{y}_{n,-k}$, given by the inverse map M^{-1}, with initial point $\mathbf{y}_{n,0} = \mathbf{y}_n$. The point $\mathbf{y}_n$ is reached by iterating n times the map M with a random displacement of amplitude ϵ at each step, starting from $\mathbf{y}_0 = \mathbf{x}_0$ (see the previous subsection). The orbit $\mathbf{y}_{n,-k}$ is obtained by iterating k times the map M^{-1} with a random displacement of the same amplitude at each step:

$$\mathbf{y}_{n,-k} = M^{-1}\left(\mathbf{y}_{n,-k+1} \right) + \epsilon \boldsymbol{\xi}_{-k} \qquad k = 1, \ldots, n \tag{14}$$

The random backward displacements $\boldsymbol{\xi}_{-k}$ are independent from the forward displacements $\boldsymbol{\xi}_{k'}$, namely, $\langle \boldsymbol{\xi}_{-k} \boldsymbol{\xi}_{k'} \rangle = 0$ and $\langle \boldsymbol{\xi}_{-k} \boldsymbol{\xi}_{-k'} \rangle = \mathrm{I}\,\delta_{kk'}$, for any $k, k' > 0$. We consider then the stochastic process $\boldsymbol{\Xi}_{n,-k}$ defined by

$$\boldsymbol{\Xi}_{n,-k} = \lim_{\epsilon \to 0} \frac{\mathbf{y}_{n,-k} - \mathbf{x}_{n-k}}{\epsilon} \qquad \boldsymbol{\Xi}_{n,-k} = DM^{-1}(\mathbf{x}_{n-k+1})\boldsymbol{\Xi}_{n,-k+1} + \boldsymbol{\xi}_{-k} \tag{15}$$

with initial condition $\boldsymbol{\Xi}_{n,0} = \boldsymbol{\Xi}_n$. The solution of the recurrence reads

$$\boldsymbol{\Xi}_{n,-k} = DM^{-k}(\mathbf{x}_n)\,\boldsymbol{\Xi}_n + \sum_{j=1}^{k} DM^{-(k-j)}\left(\mathbf{x}_{n-j} \right) \boldsymbol{\xi}_{-j} \tag{16}$$

For $k = n$, we obtain the global normalized displacement $\boldsymbol{\Xi}_n^R = \boldsymbol{\Xi}_{n,\,-n}$ after n forward and n backward iterations with noise of vanishing amplitude:

$$\boldsymbol{\Xi}_n^R = DM^{-n}(\mathbf{x}_n)\,\boldsymbol{\Xi}_n + \sum_{j=1}^{n} DM^{-(n-j)}\left(\mathbf{x}_{n-j}\right)\boldsymbol{\xi}_{-j} \tag{17}$$

Letting $\Sigma_n^{2R} = \left\langle \boldsymbol{\Xi}_n^R \left(\boldsymbol{\Xi}_n^R\right)^T \right\rangle$ be the covariance matrix, the reversibility error (RE) is defined by

$$e_n^R = \left\langle \boldsymbol{\Xi}_n^R \cdot \boldsymbol{\Xi}_n^R \right\rangle^{1/2} = \left(\mathrm{Tr}\,\Sigma_n^{2R}\right)^2 \tag{18}$$

and using Eqs. (17) and (8), an explicit expression involving only the tangent maps is obtained. Indeed the global stochastic displacement reads

$$\boldsymbol{\Xi}_n^R = \sum_{k=1}^{n} DM^{-n}(\mathbf{x}_n)\,DM^{n-k}(\mathbf{x}_k)\,\boldsymbol{\xi}_k + \sum_{k=1}^{n} DM^{-(n-k)}(\mathbf{x}_{n-k})\,\boldsymbol{\xi}_{-k}. \tag{19}$$

Taking into account the independence of $\boldsymbol{\xi}_k$ and $\boldsymbol{\xi}_{-k'}$, the expression for the reversibility error $e_n^R = \left\langle \boldsymbol{\Xi}_n^R \cdot \boldsymbol{\Xi}_n^R \right\rangle^{1/2}$ is immediately obtained.

2.4 Analytical relation between RE and LE indicators

The RE can be obtained from LE in a very simple way. We first notice that

$$DM^{-n}(\mathbf{x}_n)\,DM^{n-k}(\mathbf{x}_k) = DM^{-k}(\mathbf{x}_k) \tag{20}$$

We prove this relation by writing $M^{-n}\left(M^{n-k}(\mathbf{x})\right) = M^{-k}(\mathbf{x})$, computing the tangent map $DM^{-n}\left(M^{n-k}(\mathbf{x})\right)DM^{n-k}(\mathbf{x}) = DM^{-k}(\mathbf{x})$, and evaluating it for $\mathbf{x} = \mathbf{x}_k$. As a consequence the expression for the reversibility error becomes

$$\begin{aligned}
\left(e_n^R\right)^2 = \mathrm{Tr}\left\langle \boldsymbol{\Xi}_n^R \left(\boldsymbol{\Xi}_n^R\right)^T \right\rangle = \sum_{k=1}^{n}\Big(& \mathrm{Tr}\left[\left(DM^{-k}(\mathbf{x}_k)\right)^T\left(DM^{-k}(\mathbf{x}_k)\right)\right] + \\
& + \mathrm{Tr}\left[\left(DM^{-(n-k)}(\mathbf{x}_{n-k})\right)^T DM^{-(n-k)}(\mathbf{x}_{n-k})\right]\Big) = \\
& = 2\sum_{k=1}^{n-1}\mathrm{Tr}\left[\left(DM^{-k}(\mathbf{x}_k)\right)^T\left(DM^{-k}(\mathbf{x}_k)\right)\right] + \\
& + \mathrm{Tr}\left[\left(DM^{-n}(\mathbf{x}_n)\right)^T DM^{-n}(\mathbf{x}_n)\right] + \mathrm{Tr}\,(\mathrm{I})
\end{aligned} \tag{21}$$

Starting from $M^{-k}\left(M^k(\mathbf{x})\right) = \mathbf{x}$, computing the tangent map, and evaluating it at $\mathbf{x} = \mathbf{x}_0$, it follows that

$$DM^{-k}(\mathbf{x}_k) = \left(DM^k(\mathbf{x}_0)\right)^{-1} \tag{22}$$

Given any symplectic matrix L[3], we can prove that

[3] A symplectic matrix L is defined by $\mathrm{LJL}^T = \mathrm{J}$ where J is antisymmetric and $\mathrm{J}^2 = -\mathrm{I}$. As a consequence $\mathrm{L}^{-1} = -\mathrm{JL}^T\mathrm{J}$, and $\left(\mathrm{L}^{-1}\right)^T = -\mathrm{JLJ}$ so that $\mathrm{Tr}\left(\mathrm{L}^{-1T}\mathrm{L}^{-1}\right) = \mathrm{Tr}\left(\mathrm{JLJ}^2\mathrm{L}^T\mathrm{J}\right) = \mathrm{Tr}\left(\mathrm{LL}^T\right)$.

$$\mathrm{Tr}\left(\left(\mathrm{L}^{-1}\right)^{T}\mathrm{L}^{-1}\right)=\mathrm{Tr}\left(\mathrm{L}^{T}\mathrm{L}\right). \tag{23}$$

As a consequence in Eq. (21), we can use the following relation:

$$\mathrm{Tr}\left[\left(DM^{-k}(\mathbf{x}_k)\right)^{T}\left(DM^{-k}(\mathbf{x}_k)\right)\right]=\mathrm{Tr}\left[\left(DM^{k}(\mathbf{x}_0)\right)^{T}\left(DM^{k}(\mathbf{x}_0)\right)\right]=\left(e_k^L\right)^2. \tag{24}$$

Finally, the relation between LE and RE is given by

$$\left(e_n^R\right)^2=\sum_{k=1}^{n}\left(\left(e_k^L\right)^2+\left(e_{n-k}^L\right)^2\right)=2\left(\sum_{k=1}^{n-1}\left(e_k^L\right)^2+\frac{1}{2}\left(e_0^L\right)^2+\frac{1}{2}\left(e_n^L\right)^2\right). \tag{25}$$

This relation clearly shows how the error due to random kicks along the orbit is related to the error due to initial orthogonal kicks.

2.5 Roundoff-induced reversibility error

The reversibility error method (REM) is a very simple procedure based on n iterations of the map M followed by n iterations of the inverse map. The distance from the initial point normalized by the roundoff amplitude ϵ defines the REM error. Denoting with M_ϵ the map with roundoff, we have

$$e_n^{REM}=\left(\frac{\|M_\epsilon^{-n}\circ M_\epsilon^{n}(\mathbf{x}_0)-\mathbf{x}_0\|}{\epsilon}\right) \tag{26}$$

where ϵ is the roundoff amplitude. For the eight-byte representation of reals, we choose $\epsilon=10^{-17}$. If the map has a sufficiently high computational complexity, the displacement $\boldsymbol{\xi}$ defined by $M_\epsilon(\mathbf{x})-M(\mathbf{x})=\epsilon\boldsymbol{\xi}$ is almost random, but a unique realization is available. (For a discussion on the roundoff error, see [22]). As a consequence, the e_n^{REM} has large fluctuations, whereas e_n^R has a smooth dependence on n since it is defined by an average overall possible realizations of the stochastic displacements occurring at each iteration.

2.6 Errors for Hamiltonian flows

For Hamiltonian flows, we define the Lyapunov error $e_L(t)$ according to

$$e_L(t)=\left(\mathrm{Tr}\left(\mathrm{L}^{T}(t)\,\mathrm{L}(t)\right)\right)^{1/2} \tag{27}$$

where $\mathrm{L}(t)$ is the fundamental matrix for the tangent flow, which satisfies the linear equation $d\mathrm{L}/dt=\mathrm{JHL}$, H denotes the Hessian of the Hamiltonian computed along the orbit $\mathrm{H}_{ij}=\partial^2 H/\partial x_i\partial x_j$, and the initial condition for the matrix $\mathrm{L}(t)$ is $\mathrm{L}(0)=\mathrm{I}$. The relation with the standard fast indicators is the same as for the symplectic maps. Let $\boldsymbol{\Xi}_R(t)$ be the stochastic displacement from $\mathbf{x}_0$ after a noisy evolution up to time t and backward to $t=0$, divided by the noise amplitude ε in the limit $\varepsilon\to 0$. It has been proven [12] that $\boldsymbol{\Xi}_R(t)$ satisfies a linear Langevin equation whose solution reads

$$\boldsymbol{\Xi}^R(t)=\int_0^t \mathrm{L}^{-1}(s)\left(\boldsymbol{\xi}(s)-\boldsymbol{\xi}(s-t)\right)ds. \tag{28}$$

The reversibility error in this case is defined by the mean square deviation of the random displacement $e^R(t) = \left\langle \boldsymbol{\Xi}^R(t) \cdot \boldsymbol{\Xi}^R(t) \right\rangle^{1/2}$. As shown in [12] and from Eq. (28), we immediately obtain

$$e^R(t) = \left(2 \int_0^t \left(e^L(s) \right)^2 ds \right)^{1/2}. \tag{29}$$

If the continuous time t is replaced by an integer n and we approximate the integral with the trapezoidal rule, we recover the relation in Eq. (25) obtained for a symplectic map.

3. Integrable maps

We evaluate the errors for integrable maps with an elliptic fixed point at the origin, whose normal form is a rotation $\mathrm{R}(\Omega)$ with a frequency Ω depending on the distance from the origin. The LE asymptotic growth is linear, and oscillations are present unless the coordinates are normal. The RE asymptotic growth follows a power law n^α with exponent $\alpha = 3/2$. If the map is linear, its asymptotic growth follows a power law with $\alpha = 0$ for LE and $\alpha = 1/2$ for RE. The oscillations reflect the loss of rotational symmetry when generic coordinates are used. The roundoff induced reversibility error REM is also sensitive to the choice of coordinates, and a comparison between RE and REM is presented in the next sections.

3.1 Change of coordinate system

In generic coordinates an integrable map $M(\mathbf{x})$ is conjugated to its normal form $N(\mathbf{X})$ by a symplectic coordinate transformation $\mathbf{x} = \Phi(\mathbf{X})$; as a consequence the conjugation equation and its iterates read

$$M(\mathbf{x}) = \Phi \circ N \circ \Phi^{-1}(\mathbf{x}) \qquad M^n(\mathbf{x}) = \Phi \circ N^n \circ \Phi^{-1}(\mathbf{x}) \tag{30}$$

which imply that the orbits $\mathbf{x}_n = M^n(\mathbf{x}_0)$ and $\mathbf{X}_n = N^n(\mathbf{X}_0)$ are related by $\mathbf{x}_n = \Phi(\mathbf{X}_n)$. The tangent maps are given by

$$DM^n(\mathbf{x}_0) = D\Phi(\mathbf{X}_n) DN^n(\mathbf{X}_0) D\Phi^{-1}(\mathbf{x}_0) = D\Phi(\mathbf{X}_n) DN^n(\mathbf{X}_0) (D\Phi(\mathbf{X}_0))^{-1} \tag{31}$$

where we used $D\Phi(\mathbf{X}) D\Phi^{-1}(\mathbf{x}) = \mathrm{I}$, a relation which is proved to hold by computing the Jacobian of $\Phi \circ \Phi^{-1}(\mathbf{x}) = \mathbf{x}$. As a consequence, the expression for the Lyapunov error in both coordinate systems is

$$\begin{aligned} \left(e_n^L(\mathbf{X}_0) \right)^2 &= \mathrm{Tr} \left[(DN^n(\mathbf{X}_0))^T (DN^n(\mathbf{X}_0) \right] \\ \left(e_n^L(\mathbf{x}_0) \right)^2 &= \mathrm{Tr} \left[(DM^n(\mathbf{x}_0))^T (DM^n(\mathbf{x}_0) \right] \end{aligned} \tag{32}$$

Taking Eq. (31) into account, the last equation can be written as

$$\begin{aligned} \left(e_n^L(\mathbf{x}_0) \right)^2 &= \mathrm{Tr} \left[\mathrm{V}^{-1}(\mathbf{X}_0) (DN^n(\mathbf{X}_0))^T \mathrm{V}(\mathbf{X}_n) DN^n(\mathbf{X}_0) \right] \\ \mathrm{V}(\mathbf{X}) &= (D\Phi(\mathbf{X}))^T D\Phi(\mathbf{X}) \end{aligned} \tag{33}$$

Notice that V is a positive-defined matrix and that its determinant is equal to 1 if Φ is symplectic. For a two-dimensional map, we can write

$$\mathrm{V} \equiv \begin{pmatrix} a & b \\ b & c \end{pmatrix} \qquad \mathrm{V}^{-1} = \begin{pmatrix} c & -b \\ -b & a \end{pmatrix} \tag{34}$$

where $ac - b^2 = 1$.

3.2 Isochronous rotations: oscillations in LE and RE

If the given map is linear and two-dimensional and $M(\mathbf{x}) = \mathrm{L}\mathbf{x}$ with $|\mathrm{Tr}\,\mathrm{L}| < 2$, then the map is conjugated to a rotation $\mathrm{R}(\omega)$:

$$\mathrm{L} = \mathrm{T}\mathrm{R}(\omega)\mathrm{T}^{-1} \qquad \mathrm{R}(\omega) = \begin{pmatrix} \cos(\omega) & \sin\omega \\ -\sin(\omega) & \cos(\omega) \end{pmatrix} \tag{35}$$

Letting $\mathbf{x}_n = \mathrm{L}^n\mathbf{x}_0$ and $\mathbf{X}_n = \mathrm{R}^n\mathbf{X}_0$, the orbits in the coordinate $\mathbf{x}$ and the normal coordinate $\mathbf{X} = \mathrm{T}^{-1}\mathbf{x}$ and the Lyapunov errors are given by

$$\begin{aligned} \left(e_n^L(\mathbf{X}_0)\right)^2 &= \mathrm{Tr}\left[\mathrm{R}(-n\omega)\mathrm{R}(n\omega)\right] = 2 \\ \left(e_n^L(\mathbf{x}_0)\right)^2 &= \mathrm{Tr}\left[\mathrm{V}^{-1}\mathrm{R}(-n\omega)\,\mathrm{V}\,\mathrm{R}(n\omega)\right] \quad = 2\cos^2(n\omega) + \left(a^2 + c^2 + 2b^2\right)\sin^2(n\omega) = \\ &= \frac{(a+c)^2}{2} + \left(2 - \frac{(a+c)^2}{2}\right)\cos(2n\omega) \end{aligned} \tag{36}$$

where $\mathrm{V} = \mathrm{T}^T\mathrm{T}$, and we have used the representation given by Eq. (34) where $D\Phi = \mathrm{T}$. The error is constant in normal coordinate $\mathbf{X}$ and oscillates between 2 and $(a+c)^2 - 2 = a^2 + c^2 + 2b^2$ in the coordinate $\mathbf{x}$. The geometric interpretation is obvious since the orbits of the map belong to an ellipse rather than a circle. The result for the reversibility error is given by

$$\begin{aligned} \left(e_n^R(\mathbf{X}_0)\right)^2 &= 4n \\ \left(e_n^R(\mathbf{x}_0)\right)^2 &= 2n\,\frac{(a+c)^2}{2} + \left(2 - \frac{(a+c)^2}{2}\right) f(n) \\ f(n) &= \sum_{k=1}^{n} \left(\cos(2k\omega) + \cos(2(n-k)\omega)\right) = \cos(2n\omega) + \frac{\cos(2(n-1)\omega) - \cos(2n\omega)}{1 - \cos(2\omega)} \end{aligned} \tag{37}$$

We shall first consider the dependence of the errors on the iteration order n from $n = 1$ up to a maximum value N. Then, we shall consider the dependence on the initial condition $\mathbf{x}_0$ when it is varied on a one-dimensional grid crossing the origin for the value N of the iteration number. We choose the linear map L which depends on a single parameter λ, and its relation with the rotation frequency is

$$\mathrm{L} = \begin{pmatrix} 1-\lambda & 1 \\ -\lambda & 1 \end{pmatrix} \qquad \sin\frac{\omega}{2} = \frac{\sqrt{\lambda}}{2} \qquad 0 \le \lambda \le 4 \tag{38}$$

The rotation $\mathrm{R}(\omega)\mathbf{x}$ is the linear part for the Hénon map, whereas $\mathrm{L}\mathbf{x}$ is the linear part of the standard map that will be discussed in the next sections. The behavior of

LE and RE for these maps is provided by Eqs. (36) and (37). The error growth follows a power law with exponent $\alpha = 0$ for LE and $\alpha = 1/2$ for RE. Oscillations are present when the coordinates are not normal.

For a generic map such as L defined by Eq. (38), the growth of REM follows a power law exponent $\alpha = 1/2$ as RE, for almost any value of λ, as shown by **Figure 1**, right panel, where the plot of MEGNO corresponding to 2α is shown. The result for the map $R(\omega)$ in normal coordinates is shown in the left panel of the same figure, and the exponent is $\alpha = 1$ for almost all the values of ω.

Letting $\mathbf{X} = (X, P)^T$ and (ϕ, J) be the action angle coordinates defined by $X = (2J)^{1/2} \cos\phi$ and $P = -(2J)^{1/2} \sin\phi$, the rotation in the $\mathbf{X}$ plane becomes a translation on the cylinder:

$$\phi_n = \phi_{n-1} + \omega \mod 2\pi \qquad J_n = J_{n-1} \tag{39}$$

and in this case REM vanishes. These results show that REM strongly depends on the computational complexity of the map. The error growth always follows a power law, but, depending on the choice of the coordinates, the exponent α varies in the range $[0, 1]$. Unlike RE, we observe that REM depends linearly on the distance of the initial condition $\mathbf{x}_0$ from the origin. In **Figure 2**, we plot e_N^{REM} as a function of the initial condition when it varies on a one-dimensional grid issued from the origin for

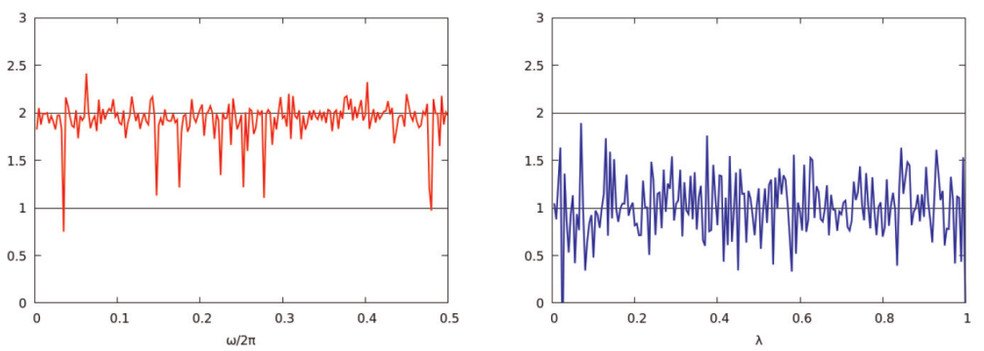

Figure 1.
Left frame: twice the asymptotic power law exponent provided by the MEGNO filter Y_N with $N = 1000$ applied to REM for a rotation $R(\omega)$ where $\omega/2\pi$ varies in the interval $[0, 1/2]$. The initial condition is $x_0 = 0.1, p_0 = 0$. Right frame: twice the asymptotic power law exponent provided by the MEGNO filter Y_N with $N = 1000$ applied to REM for a linear map L given by Eq. (38) whose parameter λ varies in $[0, 1]$. Initial condition $x_0 = 0.1, p_0 = 0$.

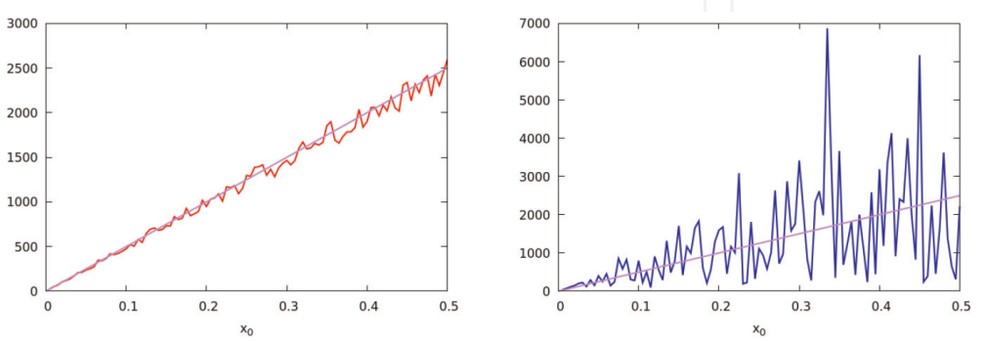

Figure 2.
Left frame: reversibility error due to roundoff e_N^{REM} for a rotation $R(\omega)$ with $\omega = 2\pi(\sqrt{2} - 1)$ and $N = 1000$ when the initial condition is varied. We choose $x_0 \in [0, 0.5], p_0 = 0$. The dependence on x_0 is evident and a linear fit $f(x_0) = 5000 x_0$ is shown, purple line. Right frame: computation of the error for the linear map with $\lambda = 4 \sin^2(\omega/2)$ where ω has the same value. The linear fit is the same.

the rotation $\mathrm{R}(\omega)$ and the linear map L. The linear dependence is evident in both cases, even though the fluctuations are large for the linear map.

3.3 Anisochronous rotations

An integrable map M in normal coordinates and the tangent map DM^n read

$$M(\mathbf{x}) = \mathrm{R}(\Omega(J))\,\mathbf{x} \qquad DM^n(\mathbf{x}) = \mathrm{R}(n\Omega) + n\Omega'\mathrm{R}'(n\Omega)\,\mathbf{x}\mathbf{x}^T \tag{40}$$

where $J = \|\mathbf{x}\|^2/2$ is the action. The square of the Lyapunov error[4] reads

$$\left(e_n^L\right)^2 = \mathrm{Tr}\left(\left(DM^n\right)^T DM^n\right) = 2 + n^2\left(2J\Omega'\right)^2 \tag{41}$$

and the square of the reversibility error is given by

$$\begin{aligned}\left(e_n^R\right)^2 = \sum_{k=1}^{n}\left(\left(e_k^L\right)^2 + \left(e_{n-k}^L\right)^2\right) &= 4n + \left(2J\Omega'\right)^2\left(\sum_{k=1}^{n}(n-k)^2 + \sum_{k=1}^{n}k^2\right)\\ &= 4n + \left(2J\Omega'\right)^2 2\left(\frac{n^3}{3} + \frac{n}{6}\right)\end{aligned} \tag{42}$$

For a fixed value of the invariant J, the slope of $\left(e_n^R\right)^2$, whose asymptotic value is 2α, is defined as $d\log\left(e_n^R\right)^2/d\log n$, and its double average is given by MEGNO $Y_n \equiv Y(e_n)$. The range of variation is [1, 3]. One can prove that for a given initial condition, the intermediate value $Y_n = 2$ is reached for

$$n = \frac{14.5}{2J|\Omega'|} = \frac{14.5}{\left(x_0^2 + p_0^2\right)|\Omega'|} \tag{43}$$

In **Figure 3**, we show the variation with $n \in [1, 1000]$ of Y_n computed for RE given by Eq. (42), corresponding to the map presented in Eq. (40), where $\Omega(J)$ is a linear function of J, and find a perfect agreement with the analytical estimate of the value of n for which the value $Y_n = 2$ is reached. In **Figure 4**, we show the variation of e_N^R and the corresponding MEGNO filter Y_N with the initial condition chosen on a one-dimensional grid crossing the origin for $N = 1000$. The integrable map is given by Eq. (40), where Ω' is constant. The error reaches a minimum value at the origin, and a similar behavior for Y_N is observed. Also e_N^{REM} decreases by approaching the origin so that the behavior is similar even though in this case the fluctuations are large. We notice that MEGNO does not eliminate the fluctuations of REM. In order to compute Y_n, one needs the sequence e_m^{REM} for $m = 1, \ldots, n$ whose computational cost is of the order of n^2. This can be avoided by storing the sequence $\mathbf{x}_{\varepsilon,m}$ and computing $\hat{e}_m{}^{REM} = \|M_\varepsilon^{-m}(\mathbf{x}_{\varepsilon,n}) - \mathbf{x}_{n-m}\|$ which turns out to be comparable with e_m^{REM}.

---

[4] The standard definition for an initial displacement along the unit vector $\boldsymbol{\eta}_0$ is $e_n^L(\boldsymbol{\eta}_0) = \|DM^n\boldsymbol{\eta}_0\|$ where $\|DM^n\boldsymbol{\eta}_0\|^2 = 1 + (n\Omega')^2\|\mathbf{x}\|^2(\boldsymbol{\eta}_0\cdot\mathbf{x})^2 + 2n\Omega'(\boldsymbol{\eta}_0\cdot\mathbf{x})(\boldsymbol{\eta}_0\cdot\mathrm{J}\mathbf{x})$ and $\mathrm{J} = \begin{pmatrix}0 & 1\\ -1 & 0\end{pmatrix}$. The sum $\left\|DM^n\begin{pmatrix}1\\0\end{pmatrix}\right\|^2 + \left\|DM^n\begin{pmatrix}0\\1\end{pmatrix}\right\|^2$ gives the Lyapunov error $\left(e_n^L\right)^2$.

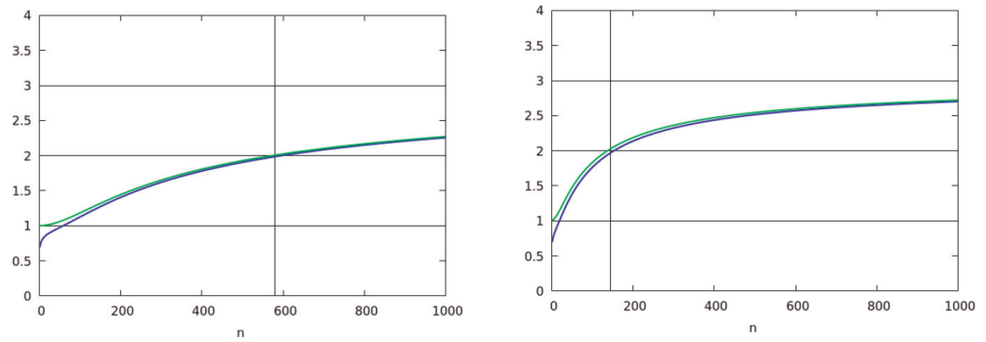

Figure 3.
Left frame: plot of MEGNO Y_n on the error e_N^R for $1 \le n \le N$ with $N = 1000$ for the integrable map with $\Omega' = 0.1$ and initial condition $x_0 = 0.5, p_0 = 0$ (blue line). The green line refers to a modified definition YM_n, where $n(loge_n^2 - loge_{n-1}^2)$ is replaced with $(loge_n^2 - loge_{n-1}^2)/(logn - log(n-1))$, which, applied to the sequence $e_n = n^\alpha$, gives 2α for any n. The vertical line gives the theoretical estimate of the value of n for which $Y_n = 2$ (see Eq. (43)) Right frame: the same for $x_0 = 1, p_0 = 0$.

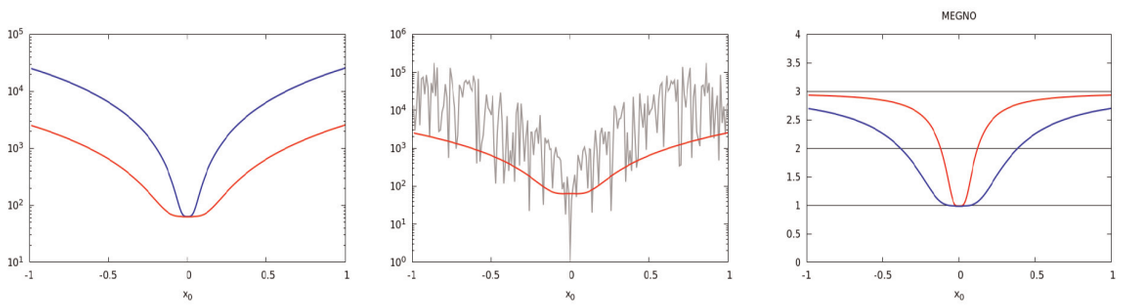

Figure 4.
Left frame: plot or the error e_N^R with $N = 1000$ for the integrable map as a function of the initial condition $x_0, p_0 = 0$ with $\Omega'(J) = 0.1$ (red line) and $\Omega'(J) = 1$ (blue line). Center frame: same plot with e_N^{REM} for $\omega = 2\pi(\sqrt{2} - 1)$ and $\Omega'(J) = 0.1$, gray line, compared with e_n^R, red line. Right frame: plot of Y_N for the integrable map with $\Omega' = 0.1$ (red line) and $\Omega'(J) = 1$(blue line).

If the coordinates are not normal, which is usually the case for a quasi integrable map, the correspondence between RE and REM is better, and it is confirmed by comparing the results for MEGNO. Just a shift of 1/2 in the exponent of the power law n^α occurs close to the origin, if the linear part is a rotation R, as for the Hénon map. If the linear part is L as for the standard map, there is no shift. The better correspondence is not surprising since the computational complexity of the map is higher when the coordinates are not normal.

4. Non-integrable maps

We examine here the behavior of the proposed dynamical indicators for two basic models, the standard map and the Hénon map.

The **standard map** is defined as a map on the torus $\mathbb{T}^2$ and reads

$$p_{n+1} = p_n - \frac{\lambda}{2\pi}\sin(2\pi x_n) \mod 1 \qquad x_{n+1} = x_n + p_{n+1} \mod 1 \qquad (44)$$

where x, p belong to the interval $[-1/2, 1/2]$ whose ends are identified. For $\lambda \ll 1$ and $|p| \gg \sqrt{\lambda}$, it is just a weakly perturbed rotator, and x, p are action angle coordinates. The origin is an elliptic fixed and very close to it; the map is approximated by a linear map

$$x_{n+1} = (1-\lambda)x_n + p_n \qquad p_{n+1} = -\lambda x_n + p_n \tag{45}$$

This map is conjugated to a rotation $\mathrm{R}(\omega)$ for $0 < \lambda < 2$ where $\sin(\omega/2) = \sqrt{\lambda}/2$. The point $x = \pm 1/2, p = 0$ is hyperbolic, and for $\lambda \ll 1$ the corresponding orbit is approximated by the separatrix of the Hamiltonian:

$$H = \frac{p^2}{2} - \frac{\lambda}{(2\pi)^2}\cos(2\pi x) \tag{46}$$

which is the interpolating Hamiltonian of the map when $\lambda \to 0$. We observe that the frequency for small oscillations is $\omega = \sqrt{\lambda}$ (see Eq. (38)) when $\lambda \to 0$. Since the time scale of the Hamiltonian H is $T = 2\pi/\sqrt{\lambda} \gg 1$, the symplectic integrator in Eq. (44), obtained for a time step $\Delta t = 1$, provides a good approximation to the orbit. Conversely, the Hamiltonian provides a good interpolation to the orbit of the map. The equation for the separatrix of H is given by

$$p = \pm\frac{\sqrt{\lambda}}{\pi}\cos(\pi x). \tag{47}$$

As a consequence, for λ small the width of the separatrix is $2\sqrt{\lambda}/\pi$. When λ increases, non-integrable features appear, such as chains of islands corresponding to resonances and a chaotic region near the separatrix due to homoclinic intersections.

The **Hénon map** is defined by

$$\begin{pmatrix} x_{n+1} \\ p_{n+1} \end{pmatrix} = \mathrm{R}(\omega)\begin{pmatrix} x_n \\ p_n + x_n^2 \end{pmatrix} \qquad \mathrm{R}(\omega) = \begin{pmatrix} \cos\omega & \sin\omega \\ -\sin\omega & \cos\omega \end{pmatrix} \tag{48}$$

Close to the origin, this is just a rotation with frequency ω. For $\omega \to 0$ this is a good symplectic integrator of the Hamiltonian:

$$H = \omega\frac{p^2 + x^2}{2} - \frac{x^3}{3} \tag{49}$$

with time step $\Delta t = 1$. The approximation is good since the characteristic time is the period of the linear rotation $T = 2\pi/\omega$. The motion is bounded by the orbit issued from the hyperbolic fixed point of the map $(x = 2\tan(\omega/2), p = -2\tan^2(\omega/2))$ which corresponds to the critical point $(x = \omega, p = 0)$ of the Hamiltonian. The stability boundary is approximated by $H(x,p) = \omega^3/6$ whose orbit explicitly reads $p = \pm(\omega - x)\sqrt{(\omega + 2x)/3}$. The Birkhoff normal forms provide an integrable approximation to the map and the corresponding interpolating Hamiltonian, from which the errors may be analytically computed.

5. The standard map

We have analyzed the errors e_n for a fixed initial condition by varying n up to a maximum value N, by varying the initial condition on a one-dimensional grid for $n = N$ and by choosing a grid in the phase plane for $n = N$. The LE shows oscillations with n, RE grows without oscillations, and the behavior of RE is similar to RE although with large fluctuations. The results obtained by filtering the errors with

MEGNO confirm this observation. In **Figure 5**, we plot the errors e_n for $\lambda = 0.1$ and $Y(e_n)$ by varying n. The fast oscillations of LE and the large fluctuations of REM are clearly visible.

When the orbit is chaotic, the growth of all errors is exponential. However, LE and RE can grow until the overflow is reached, whereas REM can grow only up to $1/\epsilon$ where ϵ is the machine accuracy. Typically in double precision, the overflow corresponds to 10^{300} where $\epsilon^{-1} \sim 10^{17}$. The same limitation is met when the Lyapunov error is computed using the shadow orbit method without renormalization rather than with the variational method. In **Figure 6**, we show the errors for a chaotic orbit when $\lambda = 0.8$. Both LE and RE exhibit an exponential growth after an initial transitory phase. The behavior of REM is very similar until $n \leq 300$. For higher values the saturation to 10^{17} is evident, and REM ceases to grow exponentially.

5.1 Initial conditions on a one-dimensional grid

Figure 7 shows the variation of LE, RE, and REM for $\lambda = 0.1$, with the initial condition chosen on a regular grid in the vertical axis p for a fixed order N. The LE oscillates when the initial condition varies, RE does not oscillate, and REM fluctuates. When the MEGNO filter is applied, LE and RE are equally smooth, whereas REM still fluctuates.

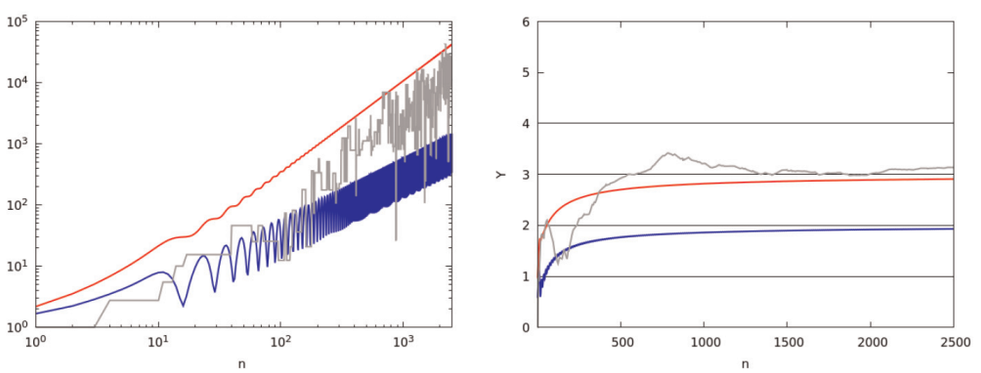

Figure 5.
Left frame: plot of the errors for the standard map with $\lambda = 0.1$ and initial condition $x_0 = 0, p_0 = 0.075$. Lyapunov error e_n^L (blue line), reversibility errors e_n^R (red line), and e_n^{REM} (gray line), for $1 \leq n \leq 2500$. Right frame: plots for the MEGNO filter Y_n for the same errors.

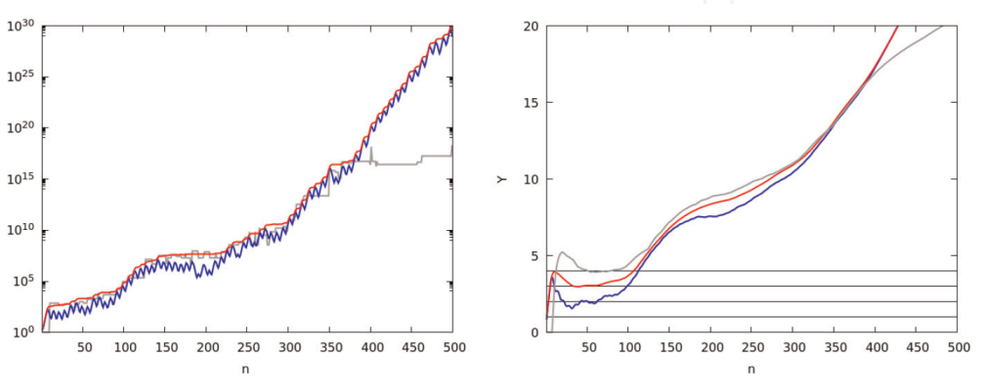

Figure 6.
Left frame: plot of the errors for the standard map with $\lambda = 0.8$ and initial condition $x_0 = 0, p_0 = 0.26$ corresponding to a chaotic orbit. Lyapunov error e_n^L (blue line), reversibility errors e_n^R (red line), and e_n^{REM} (gray line), for $n \leq 500$. Right frame: plots for the MEGNO filter Y_n for the same errors.

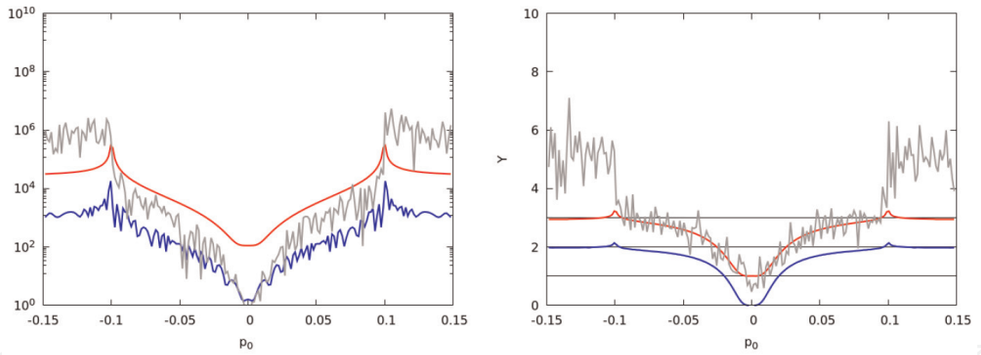

Figure 7.
Left frame: variation for the standard map with $\lambda = 0.1$ of the errors LE (blue line), RE (red line), REM (gray line) computed at $N = 1000$ with the initial condition $x_0 = 0, p_0 \in [-0.15, 1, 0.15]$. Right frame: the same for MEGNO Y_N.

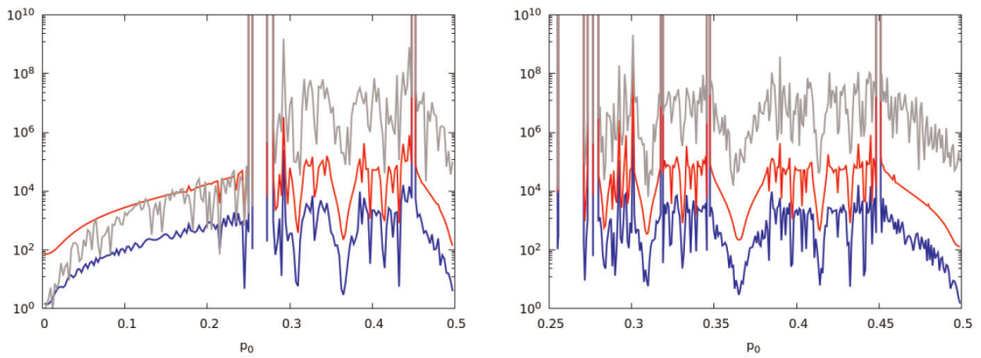

Figure 8.
Left frame: variation for the standard map with $\lambda = 0.8$ of the errors LE (blue line), RE (red line), and REM (gray line), computed at $N = 1000$ with the initial condition $x_0 = 0, p_0 \in [0, 0.5]$. Right frame: magnification in the interval $p_0 \in [0.25, 0.5]$.

In **Figure 8**, the same results are shown for a higher value of the parameter $\lambda = 0.8$ at which the dynamical structure is rich due to the presence of many resonances and small chaotic regions. The effectiveness in detecting the resonances is evident.

5.2 Initial conditions on a two-dimensional domain

We compare here LE, RE, and REM when the initial conditions are chosen in a two-dimensional phase space domain and the iteration number has a fixed value N. The most effective way of analyzing the results is to plot the errors using a logarithmic, color scale. Following the conclusions of our previous section, we show LE, RE, and REM, in a logarithmic color scale. We choose a regular two-dimensional grid in a square (or rectangular) domain of phase space with $N_g \times N_g$ points, where we compute the errors and show the result using a color scale. In order to analyze the details, smaller squares may be chosen eventually increasing the iteration number. In **Figure 9**, we show for $N = 500$ and $N_g = 200$ the color plots for the errors of the standard map with $\lambda = 0.8$ and in **Figure 10** for $\lambda = 1.5$. In the first case, the measure of chaotic orbits is small with respect to the regular ones. We observe that LE has some weak structures within the main regular component surrounding the origin, visible when the figure is sufficiently magnified. Such structures of LE, related to the oscillating growth with n, disappear when MEGNO is computed and

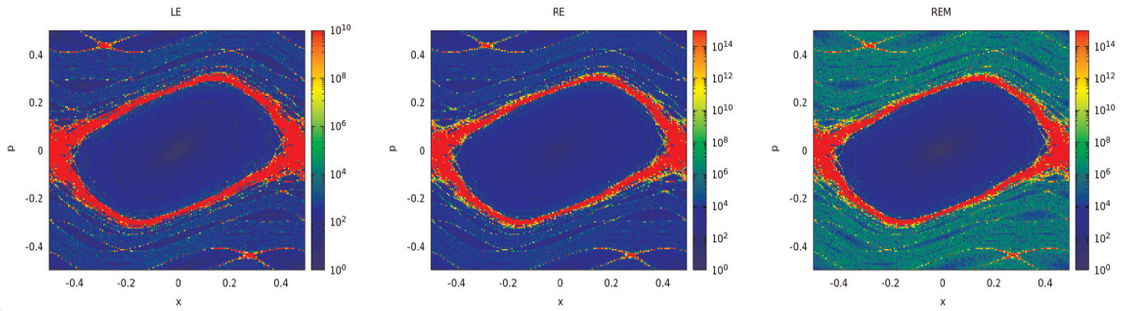

Figure 9.
Left frame: standard map with $\lambda = 0.8$ color plot of LE in a logarithmic scale for $N = 500$ and a grid with $N_g = 200$. Center frame: standard map with $\lambda = 0.8$ color plot of RE in a logarithmic scale for $N = 500$ and a grid with $N_g = 200$. Right frame: color plot of REM in a logarithmic scale.

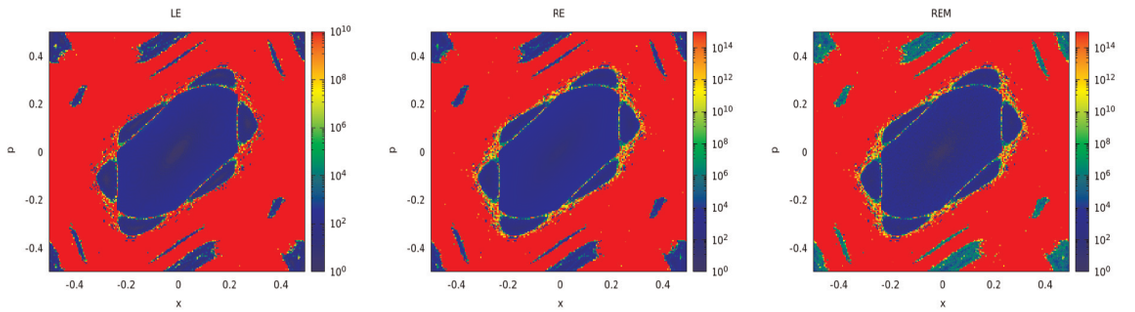

Figure 10.
Left frame: standard map with $\lambda = 0.8$ color plot of LE in a logarithmic scale for $N = 500$ and a grid with $N_g = 200$. Center frame: standard map with $\lambda = 1.5$ color plot of RE in a logarithmic scale for $N = 500$ and a grid with $N_g = 200$. Right frame: color plot of REM in a logarithmic scale.

are not present in the RE and REM plots. The spurious structures observed in FLI, which depend on the choice of the initial vector, are not present in LE, because in our definition the error does not depend on the choice of an initial displacement vector. Notice that the chosen scales have maximum equal to 10^{10} for LE and 10^{15} for RE and REM. This choice is suggested by the asymptotic behavior n^{α} of the error for regular orbits where $\alpha = 1$ for LE and $\alpha = 3/2$ for RE.

6. The Hénon map

We briefly report in this section the numerical results on the errors computed on domains of dimensions 1 and 2 in phase space. Close to the origin, the linear map in this case is a rotation $R(\omega)$. As a consequence the power law exponent of REM varies from 1 to 2, whereas the exponent for RE varies from 1/2 to 3/2. Within the main island, the variation range of the exponent for RE and REM is the same $[1/2, 3/2]$. The behavior of LE and RE close to the origin is analytically obtained by using the normal forms. The frequency $\Omega(J)$, from normal forms at the lowest order, reads

$$\Omega \simeq \omega + J\Omega_2 \qquad \Omega_2 = -\frac{1}{8}\left(3\cot\left(\frac{\omega}{2}\right) + \cot\left(\frac{3\omega}{2}\right)\right) \tag{50}$$

a formula valid for frequencies $\omega/2\pi$ not approaching the unstable resonances 0 and 1/3 where Ω_2 diverges.

In the normal coordinates (X, P), the behavior of errors is given by Eqs. (41) and (42). In the original coordinates (x, p), the error could be evaluated using Eq. (33).

In normal coordinates, the errors grow as $2J|\Omega_2|n^\alpha$ where $\alpha = 1$ for LE and $\alpha = 3/2$ for RE. When the frequency attains a low resonant value, a chain of islands appears. Close to the separatrix $J = J_s$, the frequency vanishes as $\Omega \sim 1/\log(J_s - J)$ and consequently $\Omega'(J) \sim (J_s - J)^{-1}$ as J_s is approached, up to a logarithmic correction. The errors diverge by approaching the separatrix even though the power law growth does not change except on the separatrix itself. As a consequence, LE and RE can detect the separatrix. If the remainder in the normal form interpolating Hamiltonian is taken into account, then the separatrix becomes a thin chaotic region where the errors have an exponential growth and MEGNO rises linearly with n. The REM behaves as RE neglecting its fluctuations. The Hénon map, we consider here, has a linear frequency $\omega/2\pi = 0.21$ which is close to the resonance 1/5. As a consequence a chain of five islands appears before reaching the dynamic aperture, namely, the boundary of the stability region, beyond which the orbits escape to infinity.

In **Figure 11**, we show the variation of LE, RE, and REM computed at a fixed order N and after filtering them with MEGNO, when the initial conditions are chosen on a one-dimensional grid. The resonance 1/5 is met, as shown by the appearance of a large chain of islands, since $\Omega(J)$ is monotonically decreasing. The chaotic layer at the border of the islands chain is very thin so that LE and RE grow by approaching it, as for an integrable map with a separatrix.

In **Figure 12**, we show the color plots of LE, RE, and REM in a square domain of phase space. The weakly chaotic separatrix is detectable in LE and is more clearly visible in RE. The REM plot differs from RE for the up-shit 1/2 of the power law exponent before the thin chaotic separatrix and for the presence of fluctuations.

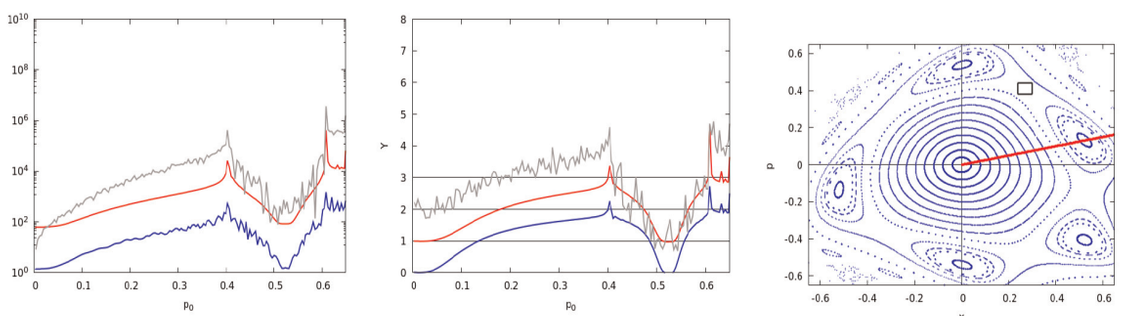

Figure 11.
Left frame: errors for the Hénon with $\omega = 0.21 \times (2\pi)$: LE (blue line), RE (red line), and REM (gray line) computed at iteration number $N = 1000$ along the line $x = r\cos\alpha$, $p = r\sin\alpha$ with $\alpha = 14^o$ joining the origin with the center of the first of five islands. Center frame: computation of MEGNO with $N = 1000$ for LE (blue line), RE (red line), and REM (gray line). Right frame: phase portrait of the Hénon map. The initial conditions for the errors in the left and right frames are chosen on the red segment.

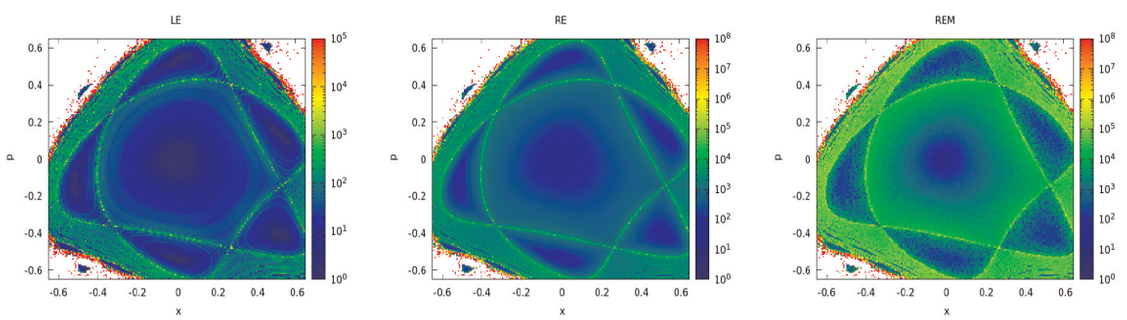

Figure 12.
Left frame: Hénon map with $\omega = 0.21 \times (2\pi)$ color plot of LE in a logarithmic scale for $N = 500$ and a grid with $N_g = 200$. The white points belong to the unstable region beyond the dynamic aperture. Center frame: color plot of RE in a logarithmic scale. Right frame: color plot of REM in a logarithmic scale.

7. Conclusions

We have presented a detailed analysis of the stability indicators LE, RE, and REM recently proposed. Defining the square of LE as the trace of the tangent map times, its transpose renders this indicator independent from the choice of an initial vector, which can introduce spurious structures. The RE is the reversibility error due to additive random noise, whereas REM is the reversibility error due to the roundoff. A very simple relation is found between RE and LE. The oscillations, which affect the fast Lyapunov indicator, can be filtered with MEGNO. Since RE has a smooth behavior and does not exhibit oscillations, filtering it by MEGNO is not necessary. The asymptotic behavior of REM is similar to RE even though it exhibits large fluctuations. The displacements caused by roundoff are almost random vectors, if the map has a high computational complexity, but since just a single realization of the process is available, the fluctuations cannot be averaged.

We have first examined the behavior of LE and RE for linear maps and for integrable maps. If the fixed point is elliptic, then the asymptotic growth follows a power law n^{α}, and the exponent does not depend on the chosen coordinates for LE and RE. Conversely, the presence of oscillations and their amplitude depends on the choice of coordinates. The growth of REM also follows a power law, but the choice of coordinates affects the exponent itself.

For a generic map which has regular and chaotic components, the error growth follows a power law and an exponential law, respectively. For the standard map and the Hénon map, the behavior of LE, RE, and REM has been compared first by varying the iteration order n up to a some value N, for a selected initial condition. Then the errors for $n = N$ have been compared when the initial point moves on a line. The theoretical predictions concerning the power law growth in the regular regions and the exponential growth in the chaotic ones are confirmed. For two-dimensional maps, the error plots for initial conditions in a rectangular domain of phase space are very similar, and the correspondence with the phase space portraits is excellent. Moreover, the different plots allow a quantitative comparison of the orbital sensitivity to initial displacements, noise, and roundoff. For maps of dimension 4 or higher, the proposed error plots on selected phase planes allow to inspect the orbital stability. Hamiltonian flows must be approximated with a high accuracy by symplectic maps, with algorithms which provide simultaneously the corresponding tangent maps [20, 21], in order to compute the errors discussed so far. A special care is required in comparing RE with REM when the chosen phase plane is invariant. Indeed given an initial point in the invariant plane, the noise brings the orbit out of it, whereas the roundoff usually does not. In this case a random kick before reversing the orbit is sufficient to bring the orbit out of the invariant plane and to restore the correspondence between REM and RE. The satisfactory results obtained so far, not only in the simple models presented here but also in high dimensional models of celestial mechanics, prove that the method we propose has a wide range of applicability.

Author details

Giorgio Turchetti[1]* and Federico Panichi[2]

1 Department of Physics and Astronomy, Alma Mater Studiorum—University of Bologna, Bologna, Italy

2 Faculty of Mathematics and Physics, Institute of Physics, University of Szczecin, Szczecin, Poland

*Address all correspondence to: giorgio.turchetti@unibo.it

References

[1] Arnold VI. The stability of the equilibrium position of a Hamiltonian system of ordinary differential equations in the general elliptic case. Soviet Mathematics Doklady. 1961;**2**: 247-249

[2] Oseledec I. A multiplicative ergodic theorem. Lyapunov characteristic numbers for dynamical systems. Transactions of the Moscow Mathematical Society. 1968;**19**:197

[3] Froeschlé C, Lega E. On the structure of symplectic mappings: The fast Lyapunov indicator: A very sensitive tool. Celestial Mechanics and Dynamical Astronomy. 2000;**78**:167

[4] Fouchard M, Lega E, Froeschlé C. On the relationship between fast Lyapunov indicator and periodic orbits for continuous flows. Celestial Mechanics and Dynamical Astronomy. 2002; **83, 205**

[5] Barrio R. Sensitivity tools vs. Poincaré sections. Chaos, Solitons & Fractals. 2005;**25**:711

[6] Skokos C. Alignment indices: A new simple method to determine the ordered or chaotic nature of orbits. Journal of Physics A: Mathematical and General. 2001;**34**:10029

[7] Skokos Ch, Antonopoulos Ch, Bountis TC, Vrahatis MN. Detecting order and chaos in Hamiltonian systems by the SALI method. Journal of Physics A: Mathematical and General. 2005;**37**: 6269-6284. Available from: https://arxiv.org/pdf/nlin/0404058.pdf

[8] Laskar J. The chaotic motion of the solar system—A numerical estimate of the size of the chaotic zones. Icarus. 1990;**88**:266

[9] Laskar J, Froeschlé C, Celletti A. The measure of chaos by numerical analysis of fundamental frequencies: Application to the standard map. Physica D. 1992; **56**:253

[10] Panichi F, Ciotti L, Turchetti G. Fidelity and reversibility in the restricted 3 body problem. Communications in Nonlinear Science and Numerical Simulation. 2015;**35**: 53-68

[11] Turchetti G, Panichi F, Sinigardi S, Vaienti S. Errors, correlations, fidelity for noisy Hamiltonian flows. Theory and numerical examples. Journal of Physics A: Mathematical and Theoretical. 2017; **50**:064001. Available from: https://arxiv.org/pdf/1509.07738.pdf

[12] Panichi F, Turchetti G. Lyapunov and reversibility errors for Hamiltonian flows. Chaos, Solitons & Fractals. 2018; **112**:83

[13] Turchetti G, Vaienti S, Zanlungo F. Asymptotic distribution of global errors in the numerical computation of dynamical systems. Physica A: Statistical Mechanics and its Applications. 2010;**389**:4994-5006

[14] Turchetti G, Vaienti S, Zanlungo F. Relaxation to the asymptotic distribution of global errors due to round off. Europhysics Letters. 2010;**89**: 40006-40010

[15] Faranda D, Mestre FM, Turchetti G. Analysis of round-off errors with reversibility test as a dynamical indicator. International Journal of Bifurcation and Chaos. 2012;**22**(09): 1-14

[16] Barrio R, Borczyk W, Breiter S. Spurious structures in chaos indicators maps. Chaos, Solitons & Fractals. 2009; **40**:1697

[17] Cincotta PM, Simo C. Simple tools to study the global dynamics in non

axisymmetric galactic potentials. Astronomy and Astrophysics Supplement Series. 2000;**147**:205

[18] Panichi F, Godziewski K, Turchetti G. The reversibility error method (REM): A new, dynamical fast indicator for planetary dynamics. Monthly Notices of the Royal Astronomical Society. 2017;**468**:469-491 https://arxiv.org/abs/1703.10596

[19] Panichi F, Turrchetti G. Birkhoff normal forms and stability indicators for betatronic motion. In: Di Mitri S, editor. NOCE Conference Proceedings. World Scientific; 2019

[20] Yoshida H. Construction of higher order symplectic integrators. Physics Letters A. 1990;**150**:262

[21] Skokos Ch, Gerlach E. Numerical integration of variational equations. Physical Review E, Statistical, Nonlinear, and Soft Matter Physics. 2010;**82**:1-19

[22] Hairer E, Lubich C, Gerhard Geometric W. Numerical Integration: Structure-Preserving Algorithms for Ordinary Differential Equations. 2nd ed. Berlin: Springer; 2006. Available from: https://cds.cern.ch/record/1250576